

Determining Rieske cluster reduction potentials

Eric N. Brown · Rosmarie Friemann · Andreas Karlsson ·
Juan V. Parales · Manon M.-J. Couture ·
Lindsay D. Eltis · S. Ramaswamy

Received: 5 March 2008 / Accepted: 29 July 2008
© SBIC 2008

Abstract The Rieske iron–sulfur proteins have reduction potentials ranging from -150 to $+400$ mV. This enormous range of potentials was first proposed to be due to differing solvent exposure or even protein structure. However, the increasing number of available crystal structures for Rieske iron–sulfur proteins has shown this not to be the case. Colbert and colleagues proposed in 2000 that differences in the electrostatic environment, and not structural differences, of a Rieske proteins are responsible for the wide range of reduction potentials observed. Using computational simulation methods and the newly determined structure of *Pseudomonas* sp. NCIB 9816-4 naphthalene

dioxygenase Rieske ferredoxin (NDO-F₉₈₁₆₋₄), we have developed a model to predict the reduction potential of Rieske proteins given only their crystal structure. The reduction potential of NDO-F₉₈₁₆₋₄, determined using a highly oriented pyrolytic graphite electrode, was -150 ± 2 mV versus the standard hydrogen electrode. The predicted reduction potentials correlate well with experimentally determined potentials. Given this model, the effect of protein mutations can be evaluated. Our results suggest that the reduction potential of new proteins can be estimated with good confidence from 3D structures of proteins. The structure of NDO-F₉₈₁₆₋₄ is the most basic Rieske ferredoxin structure determined to date. Thus, the contributions of additional structural motifs and their effects on reduction potential can be compared with respect to this base structure.

E. N. Brown · S. Ramaswamy (✉)
Department of Biochemistry,
University of Iowa,
Iowa City, IA 52242, USA
e-mail: s-ramaswamy@uiowa.edu

R. Friemann · A. Karlsson
Department of Molecular Biology,
Swedish University of Agricultural Sciences,
Biomedical Centre,
Uppsala, Sweden

J. V. Parales
Section of Microbiology,
University of California,
Davis, CA 95616, USA

M. M.-J. Couture
Medicago R&D,
1020 route de l'Eglise,
Ste-Foy, QC G1V 3V9, Canada

L. D. Eltis
Department of Microbiology and Immunology,
University of British Columbia,
Vancouver, BC V6T 1Z3, Canada

Keywords Electrochemistry · X-ray crystallography ·
Rieske ferredoxin

Introduction

Since the initial structural work by James Fee in 1984, the structures of numerous Rieske iron–sulfur cluster containing proteins have been solved—primarily by X-ray crystallography. These include the full bovine mitochondrial cytochrome *bc*₁ complex [1, 2], the chloroplast cytochrome *bc*_f complex [3], yeast cytochrome *bc*₁ complex [4], *Thermus thermophilus* Rieske protein [5], dozens of bacterial arene dioxygenase complexes [6–8], arsenite oxidase [9, 10], and the Rieske domain of SoxF from *Sulfolobus acidocaldarius* [11]. Those proteins listed in Table 1 are simple Rieske proteins—a domain containing only the Rieske cluster can be isolated from the protein.

Table 1 Crystal structures of Rieske ferredoxin proteins used in this study

Name	PDB ID
Spinach chloroplast cytochrome <i>b₆f</i> complex	1RFS
Bovine mitochondrial cytochrome <i>bc₁</i> complex	1RIE
<i>Burkholderia xenovorans</i> LB400 biphenyl dioxygenase ferredoxin	1FQT
<i>Alcaligenes faecalis</i> arsenite oxidase	1G8J
<i>Saccharomyces cerevisiae</i> cytochrome <i>bc₁</i> complex	1KB9
<i>Sulfolobus acidocaldarius</i> SoxF	1JM1
<i>Thermus thermophilus</i> Rieske protein	1NYK
<i>Sphingobium yanoikuyae</i> B1 biphenyl dioxygenase ferredoxin	2I7F
<i>Pseudomonas</i> sp. NCIB 9816-4 naphthalene dioxygenase ferredoxin	2QPZ
<i>Pseudomonas resinovorans</i> CA10 carbazole 1,9a-dioxygenase ferredoxin	1VCK
<i>Pseudomonas resinovorans</i> CA10 carbazole 1,9a-dioxygenase ferredoxin	2DE5
<i>Pseudomonas resinovorans</i> CA10 carbazole 1,9a-dioxygenase ferredoxin	2DE6
<i>Pseudomonas resinovorans</i> CA10 carbazole 1,9a-dioxygenase ferredoxin	2DE7
<i>Rhodobacter sphaeroides</i> <i>bc₁</i> complex	2NUK
<i>Rhodobacter sphaeroides</i> <i>bc₁</i> complex Y156F mutant	2NUM
<i>Rhodobacter sphaeroides</i> <i>bc₁</i> complex S154T mutant	2NVE
<i>Rhodobacter sphaeroides</i> <i>bc₁</i> complex S154C mutant	2NVF
<i>Rhodobacter sphaeroides</i> <i>bc₁</i> complex S154A mutant	2NVG
<i>Rhodobacter sphaeroides</i> <i>bc₁</i> complex Y156W mutant	2NWF

From [2, 4, 5, 7–15]

PDB Protein Data Bank

Two types of [2Fe–2S] clusters exist: plant-type clusters that are bound to the protein through four cysteines and Rieske clusters that have two histidines and two cysteines ligating the cluster. Rieske iron–sulfur clusters were initially distinguished from plant-type iron–sulfur clusters by their higher reduction potentials—up to +400 mV (versus the standard hydrogen electrode, SHE) for Rieske ferredoxins compared with approximately –500 mV for plant-type [2Fe–2S] ferredoxins. The Rieske clusters of bacterial dioxygenase systems, however, have much lower reduction potentials—for example, about –150 mV for biphenyl dioxygenase ferredoxin from *Burkholderia xenovorans* LB400 (BPDO-F_{LB400}) [13]. This large range of reduction potentials for Rieske ferredoxins (from –150 to +400 mV) was first suspected to be from different solvent accessibility to the cluster, similar to what has been seen in cytochromes [16, 17]. As structures were determined for Rieske ferredoxin proteins, however, it became apparent that there were not large variations in solvent accessibility. In fact, all Rieske

ferredoxin proteins are remarkably similar in their fold and iron–sulfur cluster locations [18].

It was proposed by Colbert et al. [13] that the electrostatic environment surrounding the iron–sulfur cluster determined the reduction potential. Observations appeared to validate this hypothesis [14, 19, 20]. In the work reported in [21, 22], site-directed mutagenesis of amino acids hydrogen bonded to the cluster sulfurs was used to probe the effect of local hydrogen bonding on the reduction potential of cytochrome *bc₁* complex Rieske ferredoxins. From these studies, a number of structures of Rieske proteins and reduction potentials are known.

Electrostatic control of reduction potentials has been examined for decades [23]. Warshel and coworkers [24, 25] devised a computational model of reduction potentials in iron–sulfur proteins with cysteine ligation. The protein dipoles–Langevin dipoles (PDL) model examined the effect of protein charges, protein dipoles, and solvent dipoles upon the relative reduction potentials of iron–sulfur proteins. They concluded that neither hydrogen bonding nor solvent accessibility could alone account for variations in reduction potential—a more complete evaluation of Coulombic interactions is necessary.

The Rieske clusters present in bacterial dioxygenase systems possess the lowest reduction potentials of all Rieske ferredoxins. The bacterial Rieske dioxygenase systems are two or three protein enzyme systems that utilize Rieske iron–sulfur clusters for shuttling electrons from a reductase to a Rieske-containing dioxygenase enzyme [7, 26]. In the three-protein systems, the first enzyme obtains two electrons from NAD(P)H. The second protein, a small soluble Rieske ferredoxin, then shuttles this electron to dioxygenase enzymes. The dioxygenase enzymes are complicated and contain three Rieske iron–sulfur clusters and three mononuclear iron active sites where the dioxygenase reaction takes place. This terminal dioxygenase enzyme is either an $\alpha_3\beta_3$ hexamer as in biphenyl dioxygenase and naphthalene dioxygenase systems or an α_3 trimer as in the carbazole 1,9a-dioxygenase system. It is because these enzymes contain a Rieske cluster that the systems are called Rieske dioxygenase systems. The second protein, however, can also contain a Rieske cluster. These Rieske ferredoxins are small proteins consisting three β -sheets with an apical Rieske iron–sulfur center. These are the Rieske proteins with reduction potentials of approximately –150 mV [27].

The structures of many Rieske dioxygenase ferredoxins are known; however, only the reduction potential of one is known—BPDO-F_{LB400} ($E'_m = -157$ mV [13, 27]). The structure of BPDO-F_{LB400} was determined in 2000. This article presents the structure and reduction potential of a second Rieske dioxygenase ferredoxin: *Pseudomonas* sp.

NCIB 9816-4 naphthalene dioxygenase ferredoxin (NDO-F₉₈₁₆₋₄).

Using computational simulation methods, and the plethora of Rieske ferredoxin structures available, we present here a model to predict the reduction potential of Rieske proteins. Using proteins with both known structures and reduction potentials, we calibrated and validated the model. The relationship between predicted reduction potential (relative to a freely solvated iron–sulfur cluster) and experimentally determined reduction potentials (relative to a normal hydrogen electrode) allows us to transform these computed reduction potentials onto the scale used by experimentalists.

Materials and methods

Pseudomonas naphthalene dioxygenase ferredoxin

NDO-F₉₈₁₆₋₄ was isolated from *Escherichia coli* cells transformed with plasmid pDTG141 containing the cloned *nahAaAbAcAd* genes encoding the naphthalene dioxygenase system [28]. Protein was purified using column chromatography as described previously using Q Sepharose and octyl Sepharose fast-flow liquid chromatography. A reddish-brown protein with spectroscopic properties identical to those of NDO-F₉₈₁₆₋₄ [29] was isolated and stored at a concentration of 30 mg/mL in 100 mM 2-morpholinoethanesulfonic acid, pH 6.8, and with 5% glycerol.

NDO-F₉₈₁₆₋₄ protein crystallized in sitting drops containing 2 μ L of the protein solution and 2 μ L of 36–38% PEG8000 and 100 mM 2-morpholinoethanesulfonic acid, pH 7.0. The crystals grew slowly at 8 °C over a period of 2 weeks. They belong to space group *P*6₁, with cell dimensions $a = b = 64.9$ Å and $c = 49.1$ Å, and with one molecule in the asymmetric unit.

Data to 2.3-Å resolution were collected using the RAXIS-IV detector mounted on a rotating copper anode generator in the laboratory. These data were used to determine the structure by molecular replacement using the program AMoRe using the polyalanine model of the biphenyl dioxygenase ferredoxin from BPDO-F_{LB400} (Protein Data Bank, PDB, ID 1FQT [13]).

A higher-resolution dataset was collected under liquid-nitrogen cryoconditions at 100 K on beamline ID14-1 at the European Synchrotron Radiation Facility, using an ADSC detector. The data were processed using programs from the Collaborative Computational Project, Number 4 (CCP4) [30]: integrated using Mosflm [31] and scaled with SCALA [32–37]. Refmac5 [38–40] and O [41, 42] were used to refine the high-resolution dataset. ARP/wARP [43–45], Coot [46], and a solvent omit-map technique were used to place water atoms [47].

Cyclic voltammetry

Cyclic voltammetry of NDO-F₉₈₁₆₋₄ was performed using a microcell essentially as described previously [27]. Briefly, cyclic voltammograms were recorded at a sweep rate of 10 mV/s with a Princeton Applied Research model 263a potentiostat using a highly oriented parallel graphite (HOPG) working electrode (Atom Graph, New York, USA) and a Ag/AgCl reference electrode (Bioanalytical Systems, West Lafayette, IN, USA). The HOPG working electrode was cleaned immediately prior to each electrochemical experiment. The protein was diluted approximately 50-fold to a concentration of 100 μ M in 20 mM 3-(*N*-morpholino)propanesulfonic acid, 80 mM KCl, pH 7.0, containing 1 mM dithiothreitol, and 2 mM neomycin to promote electron transfer between NDO-F₉₈₁₆₋₄ and the working electrode. The reduction potentials reported herein are referenced to the SHE.

Survey of Rieske protein structures

Structures of all Rieske ferredoxin proteins were downloaded from the PDB in July 2007 [48–50]. For each protein's structure, the distances from each amino acid's ionizable atoms to the closest atoms in the Rieske iron–sulfur center were calculated. When displayed graphically, the resultant plots can be used to identify residues in proximity to the Rieske cluster. In a complementary representation, schematic diagrams of the local protein environment surrounding the Rieske iron–sulfur cluster were created using a modified version of LIGPLOT [51].

All figures showing structures were created using PyMOL 0.98 [52]. Pairwise C_{α} root mean square deviation (RMSD) statistics were calculated using the Uppsala Software Factory program lsqman [53]. Structural alignments were performed by identifying corresponding C_{α} atoms between two structures. In a pairwise alignment of the two protein sequences, correspondence was defined as the two C_{α} atoms being within 10 Å of each other (using the *dp* command of Lsqman). Thus, an upper bound of 10 Å exists for all RMSD values calculated this way.

Computational reduction potential titrations

Reduction potentials for Rieske ferredoxin proteins were calculated using Gunner's multiconformational continuum electrostatics method (MCCE, version 2.2) [54, 55]. Charges used for the Rieske iron–sulfur cluster were calculated by Ullmann et al. [56] for the Rieske iron–sulfur protein found in the bovine cytochrome *bc*₁ complex. Their calculations involved only the atoms near the iron–sulfur cluster in the cytochrome *bc*₁ complex. For this study, the charges of the oxidized atoms were increased by 0.095e

and the charges of the reduced atoms were decreased by $0.095e$ so that an integral charge difference existed between the reduced and oxidized species. The ligating cysteines and histidines were singly deprotonated (lacking H_γ and $H_{\delta 1}$ protons), while all other titratable residues were present in both protonated and deprotonated states. Charges for the iron–sulfur center and ligating residues are listed in Table 2. The MCCE topology file for the Rieske cluster is available for download at <http://sil.biochem.uiowa.edu/MCCE/fes.tpl>.

The MCCE program (version 2.2) was run for each Rieske ferredoxin crystal structure in Table 1 using a protein dielectric constant of 4.0 [54, 55]. The Rieske iron–sulfur cluster reference reduction potential was set as 0 mV. Thus, all predicted reduction potentials are relative to a reference electrode in which the free iron–sulfur cluster in solvent is assigned a reduction potential of zero (and subsequently reported as E_{sim}). DelPhi (version 4.1.1) was used to determine all pairwise interaction energies between ionizable groups [57, 58]. A representative MCCE configuration file is available at http://sil.biochem.uiowa.edu/MCCE/2QPZ_A/run-12.prm.

Table 2 Charge parameterization for Rieske iron–sulfur cluster and ligating atoms used in reduction potential calculations

Component	Atom	Charge	
		Oxidized cluster	Reduced clusters
Fe ₂ S ₂	Fe ₁	0.663	0.585
	Fe ₂	0.782	0.542
	S ₁	−0.286	−0.625
	S ₂	−0.286	−0.625
Backbone	N	−0.350	−0.350
	H	0.250	0.250
	C	0.550	0.550
	O	−0.550	−0.550
	C _α	0.100	0.100
Cys	C _β	−0.080	−0.080
	S _γ	−0.920	−0.920
His	C _β	0.125	0.125
	C _γ	0.155	0.155
	N _{δ1}	−0.560	−0.560
	C _{δ2}	−0.125	−0.125
	H _{δ2}	0.125	0.125
	C _{ε1}	0.155	0.155
	H _{ε1}	0.125	0.125
N _{ε2}	−0.400	−0.400	
	H _{ε2}	0.400	0.400

The charge parameterization of the Rieske cluster was dependent upon the oxidation state of the cluster. The first column of charges is for the oxidized cluster. The second column is for the reduced cluster

Statistics

The relation between predicted and actual reduction potentials was determined using the R statistical software program [59]. The titration data produced by MCCE was first fit to the Nernst equation to determine the predicted reduction potential (versus a free Rieske cluster reference electrode). Then, all predicted/experimental reduction potential pairs were fit to a linear equation to convert predicted values (E_{sim}) to reduction potentials referenced to the normal hydrogen electrode (E_{sim}^0).

Finally, the mean-field effect of the protein environment upon the Rieske center reduction potential was calculated at the oxidized extreme of each titration. The energy of the oxidized Rieske center can be broken into three components using this approach: the interaction with the solvent, the interaction with the backbone and nonmobile residues of the protein, and the interaction with ionizable or mobile residues in the protein. The first component is the desolvation energy necessary to remove the Rieske cluster from a fully solvated state and put it into a cavity with the protein dielectric. The second and third components measure the pairwise interactions with the protein's partial charges, the third component being potentially pH dependent (although simulations were only run at neutral pH). Unlike the MCCE simulations, these components are just the average effect of the protein environment on the Rieske center at a single solution potential.

Results and discussion

NDO-F₉₈₁₆₋₄ crystal structure

The structure of NDO-F₉₈₁₆₋₄ was determined by molecular replacement using the structure of BPDO-F_{LB400}, which has 39% sequence identity. It was refined at 1.85-Å resolution with a *R* value of 15.7% (*R*_{free} = 19.7%; Table 3). The final electron density map was of good quality and all residues were visible. A metal ion was bound at the N-terminus, probably a sodium ion. All residues of the molecule are in the most favorable regions of the Ramachandran plot except for Asn-95 and Leu-96, with main chain torsion angles of 84° and −113° for Asn-95 and 121° and −79° for Leu-96. These residues have well-defined density for the backbone.

NDO-F₉₈₁₆₋₄ is an elongated molecule with approximate dimensions of 40 Å × 30 Å × 20 Å. It is essentially a β-sheet structure that belongs to a family of proteins containing Rieske iron–sulfur centers. The structures of such domains have been described as having three β-sheets, which dominate the structure [3, 13, 18, 60, 61]. This description is also relevant for NDO-F₉₈₁₆₋₄ and secondary

structure elements can be labeled as sheets A, B, or C. Sheet A consists of three strands, sheet B of four strands, and sheet C of four strands. In addition, there is a hairpin loop, which has two antiparallel hydrogen bonds (residues 42–44 and 49–51) and two short 3_{10} helix type structures (residues 9–12 and 50–54). The [2Fe–2S] center is coordinated by ligand residues in two β -hairpin structures, one that is formed by the hairpin loop (residues 42–51) and the second by a hairpin connected to sheet C, between βC_2 and βC_3 . The root mean square distance between the C_α atoms of NDO-F₉₈₁₆₋₄ and BPDO-F_{LB400} was 1.03 Å (for 102 corresponding atoms in chain A of BPDO-F_{LB400}) and 1.01 Å (for 100 corresponding atoms in chain B).

The Rieske iron–sulfur center is located on the tip of the molecule with two of the iron ligands, His-46 and His-66, exposed to the solvent (Fig. 1a). Besides these histidines,

Table 3 Summary of crystallographic data and refinement statistics for *Pseudomonas* sp. NCIB 9816-4 naphthalene dioxygenase ferredoxin (Protein Data Bank ID 2QPZ)

Space group	$P6_1$
Cell parameters	
$a = b$ (Å)	65.230
c (Å)	49.440
Resolution (Å) ^a	56.8–1.85 (1.95–1.85)
Data collection	
X-ray source	ESRF ID14-2
Wavelength (Å)	0.934
Total no. of observations	333,227
No. of unique observations	10,291
Completeness (%) ^a	99.6 (97.5)
I/σ_I ^a	8.0 (2.9)
Multiplicity ^a	14.2 (7.7)
R_{sym} ^{a,b}	0.063 (0.249)
Crystallographic refinement	
$R_{\text{factor}}/R_{\text{free}}$ (%) ^c	15.7/19.7
RMSD from ideality	
Bond lengths (Å)	0.025
Bond angles (degrees)	2.372
Mean B value (Å ²)	24.73
No. of atoms	920
No. of water atoms	98
No. of non-water heteroatoms	4

ESRF European Synchrotron Radiation Facility, RMSD root mean square deviation

^a Outer-shell values are in parentheses

^b $R_{\text{sym}} = \frac{\sum_{hkl} \sum_i |I_i(hkl) - I(hkl)|}{\sum_{hkl} \sum_i I_i(hkl)}$, where $I_i(hkl)$ is the i th measurement of reflection hkl and $I(hkl)$ is the average for that reflection

^c $R_{\text{factor}} = \frac{\sum_{hkl} ||F_{\text{obs}}| - |F_{\text{calc}}||}{\sum_{hkl} |F_{\text{obs}}|}$, where F_{obs} and F_{calc} are the observed and calculated structure factors, respectively. R_{free} is the same, but for a test set of reflections not used in refinement

which coordinate Fe₂, the second iron, Fe₁, is coordinated by Cys-44 and Cys-63. The first pair of ligands is located in a loop connected to the B β -sheet and the second pair of ligands is located in a loop of the C β -sheet. The irons are bridged by sulfide ions. The cysteine sulfurs of the ligands are hydrogen bonded to one main-chain nitrogen atom each, Cys-44 S _{γ} to His-46 N and Cys-63 S _{γ} to Leu-65 N. No hydrogen bonds are formed with the bridging sulfide ions of the Rieske cluster. Besides main-chain atoms, the iron center is surrounded by hydrophobic groups: Gly-47, Ala-49, Gly-68, Pro-81, and Val-82.

The surface around the iron center has few charged residues. Glu-62 is about 10 Å from the histidine ligands at the top of the molecule, while Asp-53 and Arg-69 are 14 Å away. Polar residues are also rare. Ser-48, Gln-67, and Thr-83 are the only polar residues within 10 Å of the exposed histidine ligands.

Rieske dioxygenase ferredoxins appear to be the smallest and simplest of the Rieske proteins examined. All other Rieske domains have additional structural elements. Bovine mitochondrial cytochrome bc_1 complex Rieske protein contains a large insertion in the second β -sheet, between the second and third strands [60]. This 30-residue insertion forms a nine-residue α -helix and a large loop. The two iron binding loops in the Rieske center of the cytochrome bc_1 fragment are connected to each other by a disulfide bridge that covers one side of the iron center. NDO-F₉₈₁₆₋₄ lacks an analogous disulfide bridge. Compared with the bc_1 complex, the Rieske domain of the spinach b_6f complex is more distorted [3]. A large α -helix is inserted prior to the second β -sheet. Likely owing to this insertion, the first strand of the first β -sheet and the first two strands of the second sheet are twisted relative to the corresponding strands in all other Rieske domains.

NDO-F₉₈₁₆₋₄ has a similar overall structure to the Rieske domain in NDO-O₉₈₁₆₋₄ (residues 38–155)—an $\alpha_3\beta_3$ Rieske dioxygenase [61]. While the Rieske iron–sulfur cluster is in the same location in the Rieske dioxygenase cluster as in the Rieske dioxygenase ferredoxins, there is an inserted loop with a helix in the cluster-binding domain (residues 118–132 in NDO-O₉₈₁₆₋₄). This loop makes subunit interactions in NDO-O₉₈₁₆₋₄ with the catalytic domain of the α -subunit. Other than this large difference, the topologies of both the cluster-binding and the basal domains are the same.

Cyclic voltammetry

Cyclic voltammetry was performed on NDO-F₉₈₁₆₋₄ using an HOPG electrode. As reported for BPDO-F_{LB400} [27], neomycin promoted stable, quasi-reversible electron transfer as judged from the shape of the cyclic voltammograms

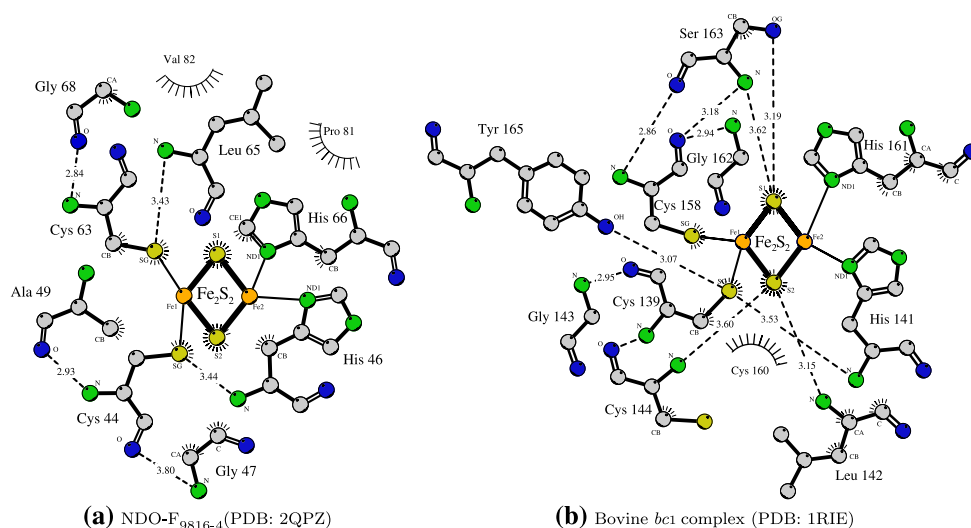


Fig. 1 The Rieszke iron–sulfur environment in *Pseudomonas* sp. NCIB 9816-4 naphthalene dioxygenase ferredoxin (*NDO-F₉₈₁₆₋₄*) and bovine cytochrome *bc₁* complex. A modified version of LIGPLOT [51] was used to create the diagrams. Colors indicate the atom's element (gray carbon, blue oxygen, green nitrogen, yellow sulfur,

orange iron). Dashes indicate potential hydrogen bonds between proton donors and acceptors (using liberal distance and angle restrictions on hydrogen bonding). Sunbursts (e.g., between S2 of the Fe_2S_2 cluster and residue Gly-47 in (a)) indicate a possible hydrophobic interaction between two atoms. *PDB* Protein Data Bank

and the separation between the anodic and cathodic peak currents (Fig. 2). The midpoint reduction potential of *NDO-F₉₈₁₆₋₄* was -150 ± 2 mV versus SHE [20 mM 3-(*N*-morpholino)propanesulfonic acid, 80 mM KCl, 2 mM neomycin, 1 mM dithiotreitol, pH 7.0, 22 °C].

Trends in Rieszke reduction potentials

Although the structure of the Rieszke iron–sulfur cluster does not differ between various Rieszke ferredoxins, the local environment in which the Rieszke iron–sulfur center differs amongst Rieszke proteins. Figure 3 shows which ionizable residues are close to the Rieszke iron–sulfur center. For ease of interpretation, the plots are arranged in order of increasing reduction potential.

It is apparent that all but the two lowest reduction potential structures have charged residues relatively close (less than 8 Å) to the Rieszke center. More importantly, there appears to be a progression of stepwise additions of ionizable residues close to the Rieszke iron–sulfur center that correlates with increased reduction potential. The first residues to be added close to the Rieszke iron–sulfur center is the pair of cysteines around 5–5.5 Å away and first seen in the arsenite oxidase structure (PDB ID 1G8J [9, 10]) with a reduction potential of +130 mV [62]. The second residue to be added is a tyrosine amino acid around 6 Å from the cluster. In the Rieszke dioxygenase ferredoxins, this residue is a phenylalanine. The third residue to be added is a serine at approximately 4.5 Å from the cluster that appears in the high-potential *bc₁* and *b_{6f}* complex structures.

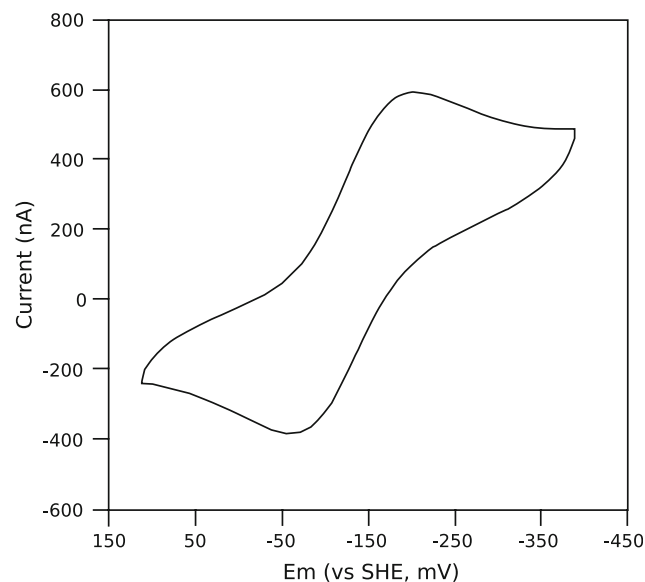
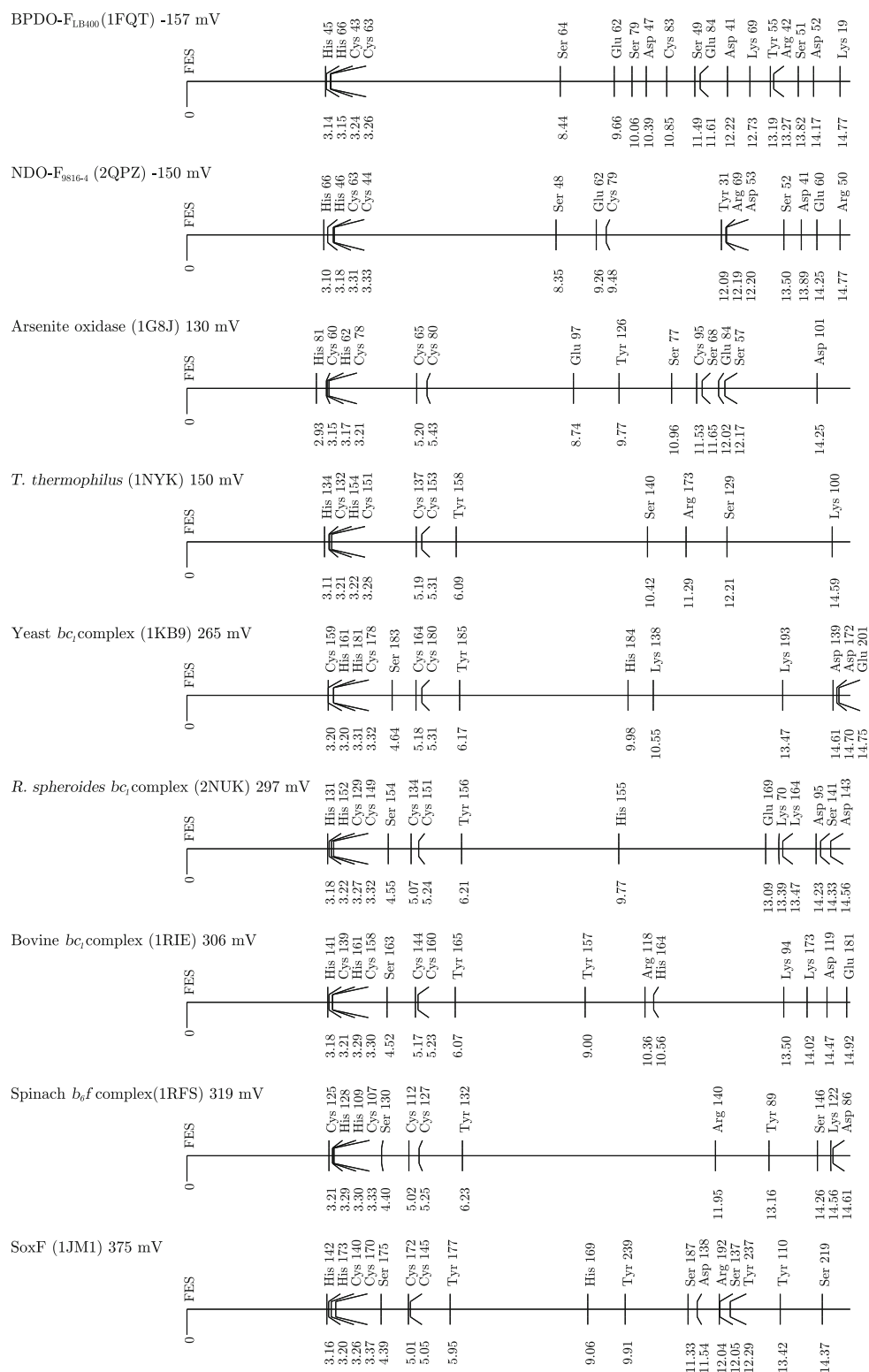


Fig. 2 Cyclic voltammogram of *NDO-F₉₈₁₆₋₄*. The sample contained 100 μM *NDO-F₉₈₁₆₋₄* in 20 mM 3-(*N*-morpholino)propanesulfonic acid, 80 mM KCl, 2 mM neomycin, 1 mM dithiotreitol, pH 7.0, 22 °C. The cyclic voltammogram was recorded at a scan rate of 10 mV/s using a highly oriented parallel graphite electrode. *SHE* standard hydrogen electrode

This progression is consistent with what was known from site-directed mutation studies of *bc₁* complex proteins. Kolling et al. [14] found that mutating this serine to alanine could reduce the reduction potential of the *Rhodobacter sphaeroides bc₁* complex by over 100 mV. Similarly, mutating the tyrosine to phenylalanine decreased the reduction potential by over 50 mV. Similar trends were

Fig. 3 Distances from ionizable atoms to Rieske iron–sulfur clusters of different reduction potential. The proteins are arranged from *top* to *bottom* in order of increasing reduction potential. As the reduction potential increases, ionizable residues appear near the Rieske cluster. *Labels above each horizontal line* indicate the residue, whereas *labels below each horizontal line* show the distance in angstroms from the ionizable atom in the amino acid side chain to the closest atom in the Rieske iron–sulfur cluster



identified in the bovine cytochrome *bc*₁ complex (although crystal structures were not employed to verify that mutations did not grossly distort the protein) [63].

Figure 1b shows the residues near the Rieske iron–sulfur cluster in the bovine cytochrome *bc*₁ complex (PDB ID

1RIE [60]). Ser-163 is forming a potential hydrogen bond between either the O_γ or the main-chain nitrogen atom of the serine with the bridging sulfur of the Rieske cluster. The main-chain nitrogen of Cys-144 is perhaps forming another hydrogen bond with the other bridging sulfur. The

other cysteine, Cys-160, does not form any hydrogen bonds with the cluster. Finally, Tyr-165 forms a hydrogen bond with the ligating sulfur of Cys-139. The situation is much simpler in NDO-F₉₈₁₆₋₄ (Fig. 1a). No residues form hydrogen bonds with the Rieske iron–sulfur cluster. The only possible hydrogen bonds to the ligating sulfurs of the cysteine are from Leu-65.

Simulated reduction potentials

The protein chains evaluated via computational reduction titrations included from 108 (for NDO-F₉₈₁₆₋₄) to 234 (for SoxF) residues (including closely bound waters and the Rieske iron–sulfur center). Each simulation required between 2,000 and 6,000 solutions to the Poisson–Boltzmann equations to compute the pairwise energies of all ionization, reduction, and rotameric states. This was by far the most time-intensive portion of the simulations. For the larger proteins, this step took approximately 7 h on a modern workstation (1.8 GHz AMD Opteron processor 244). Once the energetic interactions between different states had been determined, computing the occupancy of all states at 51 different solution potentials ranging from –1,500 to 0 mV proceeded rapidly. The resultant computed reduction potentials for the Rieske iron–sulfur center ranged from –929 to –416 mV (Table 4).

The computed reduction potentials were all less than zero, indicating that, compared with a free [Fe₂–S₂] center in solvent, which was the reference electrode for the calculations, the center in the protein preferred to be oxidized. It must be recognized that the free center, in the case of the reference potential, has the same geometry as the center in the protein. What changed upon insertion of the center into the protein are the surrounding charges and the dielectric environment—including the ligand cysteines and histidines. In this work the Rieske iron–sulfur center was composed of five independent pieces: the [2Fe–2S] core, two histidine ligands, and two cysteine ligands. Upon reduction, charges of the core atoms changed, while the histidine and cysteines remained the same as when the cluster was oxidized.

A linear model (Fig. 4) was used to relate the predicted reduction potentials (referenced relative to a free iron–sulfur cluster) to experimental reduction potentials measured relative to the normal hydrogen electrode. The quality of the fit was remarkably good ($R^2 = 0.943$). Using leave- k -out cross-validation, we determined the estimated prediction error to be 48 mV. $k = 8$ for leave- k -out cross-validation was chosen such that $\ln n \approx n/(n - k) + 1$, where n is the number of data points used in the fit (Eq. 4.5 in [68]). Shao [68] showed that this is similar to the Bayesian information criterion, which is superior to leave-one-out cross-validation.

Table 4 Computationally determined reduction potentials for Rieske ferredoxin proteins

PDB ID	Chain	Predicted		Published	
		E_{sim}	E'_{sim}	E'_m	Source
1FQT	A	–848	–115 ± 46	–157	[27]
1FQT	B	–873	–142 ± 47	–157	[27]
1G8J	B	–630	112 ± 43	130	[62]
1G8J	D	–596	147 ± 43	130	[62]
1JM1	A	–417	334 ± 44	375	[64]
1KB9	E	–578	166 ± 43	265	[65]
1NYK	A	–575	169 ± 43	150	[5]
1NYK	B	–535	210 ± 43	150	[5]
1RFS		–441	309 ± 44	319	[66]
1RIE		–454	295 ± 44	306	[67]
2DE5	D	–607	136 ± 43		
2DE5	E	–648	92 ± 43		
2DE5	F	–621	121 ± 43		
2DE6	D	–568	176 ± 43		
2DE6	E	–598	145 ± 43		
2DE6	F	–625	116 ± 43		
2DE7	D	–716	22 ± 44		
2DE7	E	–635	106 ± 43		
2DE7	F	–655	86 ± 43		
2I7F	A	–794	–59 ± 45		
2I7F	B	–879	–147 ± 47		
2NUK	A	–464	285 ± 43	297	[14]
2NUM	A	–480	268 ± 43	238	[14]
2NVE	A	–485	262 ± 43	274	[14]
2NVF	A	–476	272 ± 43	285	[14]
2NVG	A	–544	202 ± 43	170	[14]
2NWF	A	–497	250 ± 43	198	[14]
2QPZ	A	–929	–200 ± 49	–150	This study

The first column of potentials are relative to a free iron–sulfur center reference electrode. The second column of potentials are the predicted potentials from the fit in Fig. 4 relative to the normal hydrogen electrode. The last column are published reduction potentials relative to the normal hydrogen electrode

The slope of 1.04 ± 0.06 of the fit indicated that the relative differences in reduction potentials for different Rieske ferredoxin structures could be predicted using an electrostatic model with a protein dielectric constant of 4.0. Changing the protein dielectric constant to a higher value decreased the slope of the fit. However, while this fit indicated that electrostatic effects (with an associated protein dielectric constant of 4) could explain fully the differences in Rieske ferredoxin reduction potentials, the importance of this exact protein dielectric constant is likely overestimated. Other factors such as the semicovalent nature of hydrogen bonding likely play an independent role. Hence, a more complete model, independently

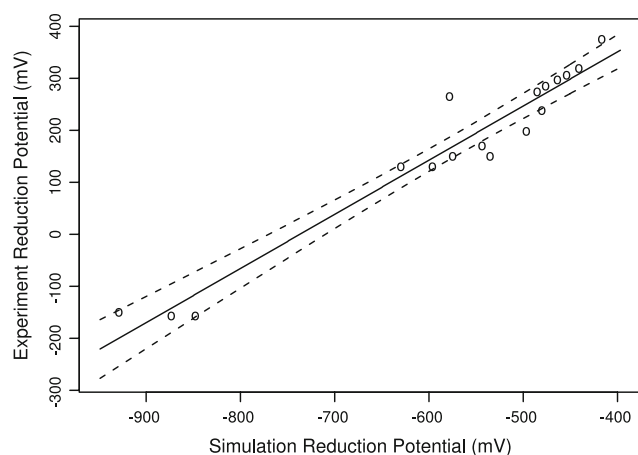


Fig. 4 Comparison of computed and experimental reduction potentials. The x-axis represents the computed reduction potential while the y-axis represents the published experimental reduction potential. Open circles show computed Rieske ferredoxin reduction potentials for seventeen structures for which experimental data exist. The solid line shows the linear fit of simulated data to experimental values, $E_m^o = (770 \pm 40 \text{ mV}) + (1.04 \pm 0.06) \times E_{\text{sim}}$, $R^2 = 0.943$. Dashed lines are 95% confidence intervals for the fit

accounting for these factors, may demand a different protein dielectric constant for an ideal fit to experimental findings.

The offset of the fit of simulated reduction potentials to experimental reduction potentials was $770 \pm 40 \text{ mV}$. This is the predicted reduction potential of the free iron–sulfur center reference electrode relative to the normal hydrogen electrode. This number could be used to adjust the reference iron–sulfur cluster reduction potential in the MCCE parameter files to calculate reduction potentials relative to the normal hydrogen electrode. This would be necessary for simulations with more than one type of redox-active center such as is found in the greater bc_1 complex (containing cytochrome and quinone ligands) and terminal dioxygenase enzyme (with the ferrous or ferric catalytic non-heme iron)—all reference reduction potentials in the simulation must be on the same scale.

The calculated reduction potential was decomposed into three energy components using the mean-field approach: a desolvation energy term (E_{dsol}), a term quantifying the interaction energy between the Rieske center and static backbone atoms (E_{bkb}), and finally an energy term for the Rieske center interacting with amino acid side chains (E_{side}). The first two of these energy terms were independent of the pH or solution reduction potential. The third, however, involved the average state of the protein at a given pH and solution potential. In any one microstate a side chain was protonated or deprotonated and took one of many conformations. The mean-field pairwise energy term used a weighted average of the interaction energies of each

of these microstates with the Rieske center (the weight being the occupancy of the microstate in the simulation at the given solution potential and pH). Owing to this averaging, the sum of these three energy terms approximated the final calculated reduction potential: $E_{\text{sim}} \approx E_{\text{dsol}} + E_{\text{bkb}} + E_{\text{side}}$. In this sum $E_{\text{dsol}} \approx 200 \pm 20 \text{ mV}$, $E_{\text{bkb}} \approx 510 \pm 130 \text{ mV}$, and $E_{\text{side}} \approx -1,340 \pm 50 \text{ mV}$; thus, the relative importance of these three terms was $E_{\text{dsol}} < E_{\text{bkb}} < E_{\text{side}}$.

The linear fit of the three mean-field energy terms to experimental reduction potentials, E_m^o , was used to identify important terms:

$$E_m^o \approx (-5 \pm 3) \times E_{\text{dsol}} + (1.5 \pm 0.3) \times E_{\text{bkb}} + (1.1 \pm 0.2) \times E_{\text{side}} + C$$

The importance of the desolvation term was minor for describing the relative reduction potentials of Rieske clusters (it was not significantly different from zero, $P = 0.14$). This term was also of minor importance in determining the absolute reduction potential for these Rieske clusters. This is understandable since all Rieske ferredoxins have a Rieske [2Fe–2S] center in the same location at the end of an approximately prolate spheroid protein. Thus, the protein dielectric cavity into which the Rieske iron–sulfur cluster was placed was not significantly different for the various Rieske proteins and was similar to a fully solvated iron–sulfur cluster. The similarity was also reflected in the small variance of the E_{dsol} term: $\sigma_{\text{dsol}} = 20 \text{ mV}^2$. The other two energy terms were more important since they have a nonzero relation to the experimental reduction potential (each significantly different from zero, $P < 0.01$).

If proteins are found that contain a Rieske cluster buried inside the protein, the relevance of the desolvation term is expected to increase. For example, this may be an important factor in the bc_1 complex where the Rieske cluster alternates between a position next to the desolvated ubiquinone site (Q_o) and the cytochrome c_1 site. Another example may be in the Rieske dioxygenase enzymes. When the small Rieske dioxygenase ferredoxin binds to the larger dioxygenase enzyme, the desolvation of the ferredoxin's Rieske cluster and the dioxygenase's related Rieske cluster will likely increase the reduction potential of the two clusters. The relative increase of the difference between the potentials of these two clusters could impact how efficiently the electron is passed from the ferredoxin's Rieske center to the dioxygenase's Rieske center.

Series of *R. sphaeroides* mutations

The series of mutant *R. sphaeroides* bc_1 complexes for which both structures and experimental reduction potentials

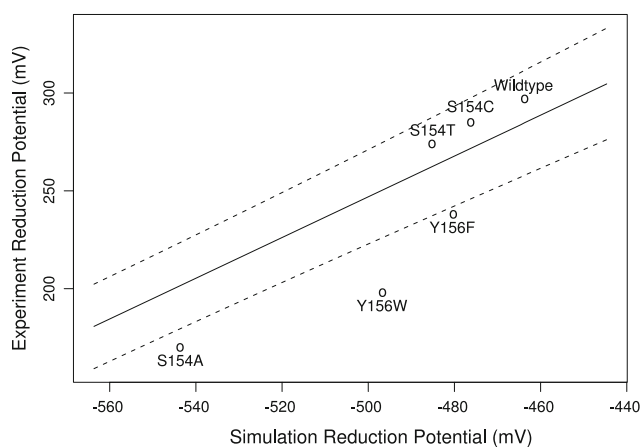


Fig. 5 Comparison of computed and experimental reduction potentials for six structures of the *Rhodobacter sphaeroides* bc_1 complex. The x-axis represents the computed reduction potential, while the y-axis represents the published experimental reduction potential. The solid line shows the linear fit of simulated data to experimental values, $E_m' = (770 \pm 40 \text{ mV}) + (1.04 \pm 0.06) \times E_{sim}$. Dashed lines are 95% confidence intervals for the fit

exist presented an opportunity to test the precision of the MCCE program. Figure 5 is a close-up view of Fig. 4 showing the relevant simulated and experimental data. The overall effects of the mutations were reasonably well predicted—the correlation between predicted and actual reduction potential was 88.5%. The method, however, incorrectly predicted that the Y156F mutant bc_1 complex had a reduction potential greater than the S154T mutant. The predicted reduction potential was also overestimated for the two tyrosine mutants and the S154A mutant by approximately 30 mV. In those three cases, a hydrogen bond present in the wild-type protein was lacking in the mutant protein. Thus, the predicted difference between the S154A mutant's and the wild type's reduction potentials was only 83 mV, whereas experimentally a difference of 114 mV has been observed [14]. It therefore appears that the prediction method underweights the importance of hydrogen bonds. This could be due to the partial covalent nature of hydrogen bonds that is not accounted for in the electrostatics calculations of interaction energies.

From the mean-field decomposition of the reduction potential for the wild-type *R. sphaeroides* bc_1 complex, the two most important residues (outside the covalently bonded cysteines and histidines) were Ser-154 and Tyr-156. The serine was predicted to raise the reduction potential by 68 mV (relative to the given side chain being absent). Ser-154 was directly hydrogen bonded to the bridging sulfur in the Rieske iron–sulfur cluster. The tyrosine had a more moderate effect of only raising the potential by 24 mV. Unlike Ser-154, Tyr-156 is hydrogen bonded to the S_γ atom of Cys-129, one of the ligands covalently bonded to the Rieske iron–sulfur cluster.

Predicted reduction potentials for *Pseudomonas resinovorans* CA10 carbazole 1,9a-dioxygenase ferredoxin and *Sphingobium yanoikuyae* B1 biphenyl dioxygenase ferredoxin

One major potential use for the MCCE method of computing protein reduction potentials is the analysis of protein structures for which no experimental reduction potentials are available. Using the derived relationship between calculated reduction potentials (referenced to the free iron–sulfur cluster) and experimental reduction potentials (referenced to the normal hydrogen electrode), the reduction potentials for new Rieske ferredoxin structures can be estimated. Two Rieske dioxygenase ferredoxin proteins were analyzed in an attempt to predict their reduction potentials: *Sphingobium yanoikuyae* B1 biphenyl dioxygenase ferredoxin (BPDO- F_{B1}) and *Pseudomonas resinovorans* CA10 carbazole 1,9a-dioxygenase ferredoxin (CARDO- F_{CA10}). BPDO- F_{B1} is the Rieske ferredoxin associated with an $\alpha_3\beta_3$ Rieske dioxygenase system [7], while CARDO- F_{CA10} is the ferredoxin from an α_3 Rieske dioxygenase system [8]. The predicted reduction potentials are presented in Table 5. Two noncrystallographically identical structures for BPDO- F_{B1} (PDB ID 2I7F [7]) and nine for CARDO- F_{CA10} (PDB ID 2DE5 [8]) have been published.

Using the two available structures for BPDO- F_{B1} , the best estimate for the reduction potential was -100 ± 78 mV. Since neither of the independent structures for BPDO- F_{B1} can be deemed superior to the other, the average simulated potential is used as the best estimate. This was similar but slightly higher in potential than NDO- F_{9816-4} and BPDO- F_{LB400} . Unlike those two ferredoxins, BPDO- F_{B1} had a polar cysteine residue, Cys-83, close to the Rieske cluster and may be interacting with one of the bridging sulfurs. According to the mean-field analysis, this

Table 5 Predicted reduction potentials for Rieske ferredoxins based on computer reduction titration simulations

Protein	PDB ID	Predicted E_{sim}'
CARDO- F_{CA10}	2DE5	116 ± 48
	2DE6	145 ± 52
	2DE7	72 ± 62
BPDO- F_{B1}	2I7F	-100 ± 78

Reduction potentials are reported relative to the normal hydrogen electrode. Potentials were first predicted using the methods described in the text relative to the free iron–sulfur cluster reference electrode and then converted for reference to the normal hydrogen electrode (reported here) using the linear fit in Fig. 4. Errors were estimated using the confidence intervals of the linear fit

CARDO- F_{CA10} *Pseudomonas resinovorans* CA10 carbazole 1,9a-dioxygenase ferredoxin, BPDO- F_{B1} *Sphingobium yanoikuyae* B1 biphenyl dioxygenase ferredoxin

residue contributed to a 24–37-mV increase in the reduction potential.

The best estimate for the reduction potential of CARDO- F_{CA10} was 116 ± 48 mV for CARDO- F_{CA10} in complex with CARDO- O_{J3} (PDB ID 2DE5), 145 ± 52 mV for the reduced complex (PDB ID 2DE6), and 72 ± 62 mV for the complex with carbazole bound (PDB ID 2DE7). Since all structures of CARDO- F_{CA10} were extremely similar (the RMSD of 104 C_α atoms was less than 0.6 Å for all 24 pairs of CARDO- F_{CA10} structures) and most of the differences were localized to the end of the protein farthest away from the Rieske cluster, it was likely that one reduction potential should be used to describe all CARDO- F_{CA10} structures: the average predicted reduction potential was thus 110 ± 61 mV. Compared with the five other Rieske dioxygenase ferredoxin structures that were analyzed, these nine had interaction energies with the backbone, E_{bb} , almost 200 mV higher in energy (500 ± 20 vs. 300 ± 60 mV). Neither the desolvation energies nor the total interaction energy with the side chains differed (184 ± 8 vs. 190 ± 13 mV and $-1,310 \pm 40$ vs. $-1,360 \pm 60$ mV, respectively).

The difference in reduction potentials of CARDO- F_{CA10} , BPDO- F_{LB400} , and NDO- F_{9816-4} Rieske proteins may indicate a difference in electrochemical properties of electron carriers associated with the different classes of dioxygenase enzymes. The carbazole 1,9a-dioxygenase system supplies electrons to a timeric α_3 dioxygenase enzyme. The biphenyl dioxygenase and naphthalene dioxygenase systems, on the other hand, have hexameric $\alpha_3\beta_3$ dioxygenase components. The two ferredoxin proteins known to associate with $\alpha_3\beta_3$ dioxygenase enzymes have significantly lower reduction potentials than that calculated for the ferredoxin associating with an α_3 dioxygenase enzyme. This may be a general feature subdividing the Rieske dioxygenase systems; however, additional reduction potentials and structures need to be determined to address this hypothesis.

Limitations and potential improvements

Rieske iron–sulfur proteins can currently be split into two sets: the high-potential proteins and the low-potential proteins. The low-potential Rieske ferredoxin set is composed of Rieske dioxygenase ferredoxins, while all other Rieske ferredoxins have higher reduction potentials. The computational modeling presented in this work accurately predicts the separation of these two classes of Rieske proteins. Resolving the differences in reduction potentials amongst the low-potential Rieske dioxygenase ferredoxins is currently hindered by the dearth of experimentally determined reduction potentials available. The determination of additional reduction potentials for Rieske dioxygenase ferredoxins will hopefully validate and improve this computational model.

In addition to the reduction–oxidation properties of Rieske iron–sulfur clusters, the two ligating histidines can undergo deprotonation at high pH [20]. While at the moderate pH used in these simulations both histidines are protonated, at a higher pH the behaviors of Rieske ferredoxins are expected to differ. Zu et al. [20] found that low-potential Rieske BPDO- F_{LB400} had histidine pK_a values appreciably higher than those observed in bc_1 complex Rieske ferredoxins. Refinements to the MCCE parameters for the Rieske cluster should be able to capture the linked deprotonation and reduction behavior of Rieske ferredoxins. However, unlike the current parameterization that has two states (reduced and oxidized), the revised parameters would require six states (reduced and oxidized, each with protonated, singly deprotonated, and doubly deprotonated substates). Each state would require partial charge assignment for all Rieske cluster and ligating residue atoms in addition to pK_a and E_m assignments.

A complete model describing reduction and deprotonation, however, would first be applicable only to high-potential Rieske proteins for which sufficient electrochemistry and pK_a data are available. Low-potential dioxygenase proteins could be included in the model as additional reduction potential and pK_a measurements are published. Given the simple nature of the NDO- F_{9816-4} protein, it may be an ideal framework with which to measure the effects of protein mutations on reduction potential.

One benefit of the MCCE formalism over the PDL method used by Warshel [24, 25] is its combined treatment of ionization and reduction [69]. The PDL method, however, includes a more realistic solvent model [70, 71]. By treating the solvent as a microscopic collection of dipoles, the Lavgevin dipole solvent model more closely represents an all-atom solvent model than the macroscopic dielectric medium used by MCCE. The more advanced PDL/S-LRA (semimacroscopic protein dipoles-Langevin dipoles method with linear response approximation) method used by Warshel expands the PDL method by averaging over protein configurations determined from molecular dynamics simulations. While the MCCE method samples alternate side chain positions, molecular dynamics could be used with MCCE to sample alternate backbone conformations. The use of multiple independent CARDO- F_{CA10} structures in the calculation of its reduction potential is an incomplete, coarse approximation of rigorous molecular dynamics of the protein backbone.

For future iron–sulfur protein reduction potential calculations, either Gunner's MCCE or Warshel's PDL methods could be used. A side-by-side comparison of the MCCE and PDL methods may be of interest to the computational biophysics community. High-level ab initio

quantum mechanical treatment of reduction potentials still has a place [56]. In addition to being a prerequisite for both MCCE and PDL parameterizations, these studies can give absolute reduction potentials rather than just comparing the relative potentials of two similar proteins. More importantly, these methods can account for the electronic characteristics of iron–sulfur clusters, including the anti-ferromagnetic coupling (and hence opposite spin) of the two iron atoms in the Rieske cluster [56, 72]. These benefits, however, are hampered by the vast time and computational resources required.

Conclusion

NDO-F₉₈₁₆₋₄ is proposed to be the simplest Rieske ferredoxin reported to date. Other Rieske proteins can be described in terms of changes, additions, and insertions into this base structure. Cyclic voltammetry determined the reduction potential of NDO-F₉₈₁₆₋₄ to be -150 mV versus the SHE.

In addition to presenting the structure of NDO-F₉₈₁₆₋₄, we have developed a method for computing the reduction potentials of Rieske ferredoxin proteins given only their structure. This method accurately predicts the reduction potentials of 17 Rieske proteins for which both structures and experimentally determined potentials exist. Additionally, it has a bright future for *in silico* prediction of the effects of mutations on Rieske protein reduction potentials and estimating reduction potentials for newly determined Rieske ferredoxin structures. Additional work is necessary, however, for this method to be applied to systems containing multiple redox-active sites such as the large *bc*₁ complex and Rieske dioxygenase system ferredoxin–dioxygenase complexes.

Acknowledgments We thank Dan Ferraro, Adam Okerlund, Lokesh Gakhar, Chi-Li Yu, Johna Leddy, David Gibson, and Hans Eklund for their support, ideas, and assistance. We thank Elizabeth Kamp for her assistance in editing this manuscript. We would like to thank the Macromolecular Crystallography Group beamline ID14-1 at the European Synchrotron Radiation Facility for help with data collection. E.B. is a University of Iowa MSTP trainee and would like to acknowledge financial support through a fellowship from the University of Iowa Center for Biocatalysis and Bioprocessing. M.M.J.C. was the recipient of a studentship from the FCAR of Quebec, Canada. S.R. would like to acknowledge financial support from USPHS grant no. GM62904. This work was supported in part by a Discovery grant from the Natural Sciences and Engineering Research Council (NSERC) of Canada (to L.D.E.).

References

- Xia D, Yu CA, Kim H, Xia JZ, Kachurin AM, Zhang L, Yu L, Deisenhofer J (1997) *Science* 277:60–66
- Iwata S, Lee JW, Okada K, Lee JK, Iwata M, Rasmussen B, Link TA, Ramaswamy S, Jap BK (1998) *Science* 281:64–71
- Carrell CJ, Zhang H, Cramer WA, Smith JL (1997) *Structure* 5:1613–1625
- Lange C, Nett JH, Trumppower BL, Hunte C (2001) *EMBO J* 20:6591
- Hunsicker-Wang LM, Heine A, Chen Y, Luna EP, Todaro T, Zhang YM, Williams PA, Mcree DE, Hirst J, Stout CD, Fee JA (2003) *Biochemistry* 42:7303
- Ferraro D, Gakhar L, Ramaswamy S (2005) *Biochem Biophys Res Commun* 338:175–190
- Ferraro DJ, Brown EN, Yu CL, Parales RE, Gibson DT, Ramaswamy S (2007) *BMC Struct Biol* 7:10
- Ashikawa Y, Fujimoto Z, Noguchi H, Habe H, Omori T, Yamane H, Nojiri H (2006) *Structure* 14:1779–1789
- Ellis PJ, Conrads T, Hille R, Kuhn P (2001) *Structure* 9:125–132
- Anderson GL, Williams J, Hille R (1992) *J Biol Chem* 267:23674
- Bönisch H, Schmidt CL, Schaefer G, Landstein R (2002) *J Mol Biol* 319:791
- Carrell CJ, Zhang H, Cramer WA, Smith JL (1997) *Structure* 5:1613
- Colbert CL, Couture MMJ, Eltis LD, Bolin JT (2000) *Structure* 8:1267–1278
- Kolling DJ, Brunzelle JS, Lhee S, Crofts AR, Nair SK (2007) *Structure* 15:29–38
- Nam J, Noguchi H, Fujimoto Z, Mizuno H, Ashikawa Y, Abo M, Fushinobu S, Kobashi N, Wakagi T, Iwata K, Yoshida T, Habe H, Yamane H, Omori T, Nojiri H (2005) *Proteins* 58:779–789
- Stellwagen E (1978) *Nature* 275:73–74
- Schlauder GG, Kassner RJ (1979) *J Biol Chem* 254:4110–4113
- Meyer J (2008) *J Biol Inorg Chem* 13:157–170
- Zu Y, Bernardo SD, Yagi T, Hirst J (2002) *Biochemistry* 41:10056–10069
- Zu Y, Couture M, Kolling D, Crofts A, Eltis L, Fee J, Hirst J (2003) *Biochemistry* 42:12400–12408
- Schröter T, Hatzfeld OM, Gemeinhardt S, Korn M, Friedrich T, Ludwig B, Link TA (1998) *Eur J Biochem* 255:100–106
- Denke E, Merbitz-Zahradnik T, Hatzfeld OM, Snyder CH, Link TA, Trumppower BL (1998) *J Biol Chem* 273:9085–9093
- Moore GR, Pettigrew GW, Rogers NK (1986) *Proc Natl Acad Sci USA* 83:4998–4999
- Langen R, Jensen GM, Jacob U, Stephens PJ, Warshel A (1992) *J Biol Chem* 267:25625–25627
- Stephens PJ, Jollie DR, Warshel A (1996) *Chem Rev* 96:2491–2513
- Bugg TD, Ramaswamy S (2008) *Curr Opin Chem Biol* 12:1–7
- Couture MMJ, Colbert CL, Babini E, Rosell FI, Mauk AG, Bolin JT, Eltis LD (2001) *Biochemistry* 40:84–92
- Suen WC (1991) Genetic and biochemical studies of the ferredoxin TOL component of toluene dioxygenase from *Pseudomonas putida* FI. University of Iowa, Iowa City
- Haigler BB, Gibson DT (1990) *J Bacteriol* 172:465–468
- Collaborative Computational Project Number 4 (1994) *Acta Crystallogr D Biol Crystallogr* 50:760–763
- Powell HR (1999) *Acta Crystallogr D Biol Crystallogr* 55:1690–1695
- Evans PR (1993) In: Data collection and processing. CCP4 study weekend, pp 114–122
- Read RJ (1999) *Acta Crystallogr D Biol Crystallogr* 55:1759–1764
- Hamiltona, Rollett, Sparks (1965) *Acta Crystallogr* 18:129–130
- Diederichs K, Karplus PA (1997) *Nat Struct Biol* 4:269–275
- Weiss M, Hilgenfeld R (1997) *J Appl Crystallogr* 30:203–205
- Weiss M (2001) *J Appl Crystallogr* 34:130–135
- Murshudov G, Vagin A, Dodson E (1996) In: The refinement of protein structures. CCP4 study weekend, pp 93–104

39. Murshudov GN, Vagin AA, Dodson EJ (1997) *Acta Crystallogr D Biol Crystallogr* 53:240–255
40. Pannu NJ, Murshudov GN, Lebedev A, Vagin AA, Wilson KS, Dodson EJ (1999) *Acta Crystallogr D Biol Crystallogr* 55:247–255
41. Jones TA, Zou JY, Cowan SW, Kjeldgaard M (1991) *Acta Crystallogr A* 47:110–119
42. Kleywegt GJ, Zou JY, Kjeldgaard M, Jones TA (2001) In: Rossmann MG, Arnold E (eds) *International tables for crystallography*. Kluwer Academic Publishers, Dordrecht, pp 353–356, 366–367
43. Lamzin VS, Wilson KS (1993) *Acta Crystallogr D Biol Crystallogr* 49:129–147
44. Lamzin VS, Wilson KS (1997) In: Carter C, Sweet B (eds) *Methods in enzymology*. Academic Press, San Diego, pp 269–305
45. Lamzin VS, Perrakis A, Wilson KS (2001) In: Rossmann MG, Arnold E (eds) *International tables for crystallography*, vol F. Kluwer Academic Publishers, Dordrecht, pp 720–722
46. Emsley P, Cowtan K (2004) *Acta Crystallogr D Biol Crystallogr* 60:2126–2132
47. Brown EN (2009) *Rieske business: Rieske metal clusters in Rieske ferredoxins and Rieske dioxygenases*. University of Iowa, Iowa City
48. Bernstein FC, Koetzle TF, Williams GJB, Meyer JEF, Brice MD, Rodgers JR, Kennard O, Shimanouchi T, Tasumi M (1977) *J Mol Biol* 112:535–542
49. Berman HM, Westbrook J, Feng Z, Gilliland G, Bhat TN, Weissig H, Shindyalov IN, Bourne PE (2000) *Nucleic Acids Res* 28:235–242
50. Berman HM, Henrick K, Nakamura H (2003) *Nat Struct Biol* 10:980
51. Wallace AC, Laskowski RA, Thornton JM (1995) *Protein Eng* 8:127–134
52. DeLano WL (2000) *The PyMOL molecular graphics system*, version 0.98. DeLano Scientific, San Carlos
53. Kleywegt GJ, Jones TA (1994) A super position. Biomedical Centre, Uppsala University, Sweden
54. Alexov E, Gunner M (1997) *Biophys J* 74:2075–2093
55. Georgescu RE, Alexov EG, Gunner MR (2002) *Biophys J* 83:1731–1748
56. Ullmann GM, Noodleman L, Case DA (2002) *J Biol Inorg Chem* 7:632–639
57. Rocchia W, Alexov E, B H (2001) *J Phys Chem B* 105:6507–6514
58. Rocchia W, Sridharan S, Nicholls A, Alexov E, Chiabrera A, Honig B (2002) *J Comp Chem* 23:128–137
59. R Development Core Team (2006) *R: A language and environment for statistical computing*. R Foundation for Statistical Computing, Vienna
60. Iwata S, Saynovits M, Link TA, Michel H (1996) *Structure* 4:567–579
61. Kauppi B, Lee K, Carredano E, Parales RE, Gibson DT, Eklund H, Ramaswamy S (1998) *Structure* 6:571–586
62. Hoke KR, Cobb N, Armstrong FA, Hille R (2004) *Biochemistry* 43:1667–1674
63. Leggate EJ, Hirst J (2005) *Biochemistry* 44:7048–7058
64. Schmidt CL, Hatzfeld OM, Petersen A, Link TA, Schafe G (1997) *Biochem Biophys Res Commun* 234:283–287
65. Merbitz-Zahradnik T, Zwicker K, Nett J, Link T, Trumpower B (2003) *Biochemistry* 42:13637–13645
66. Zhang H, Carrell CJ, Huang D, Sled V, Ohnishi T, Smith JL, Cramer WA (1996) *J Biol Chem* 271:31360–31366
67. Link TA, Saynovits M, Assmann C, Iwata S, Ohnishi T, von Jagow G (1996) *Eur J Biochem* 237:71–75
68. Shao J (1997) *Statistica Sinica* 7:221–264
69. Gunner MR, Alexov E (2000) *Biochim Biophys Acta* 1458:63–87
70. Warshel A, Papazyan A (1998) *Curr Opin Struct Biol* 8:211–217
71. Warshel A, Sharma PK, Kato M, Parson WW (2006) *Biochim Biophys Acta* 1764:1647–1676
72. Noodleman L, Normal JGJ, Osborne JH, Aizman A, Case DA (1985) *J Am Chem Soc* 107:3418–3426